

4. D. W. Keith, C. R. Ekstrom, Q. A. Turchette, D. E. Pritchard, *Phys. Rev. Lett.* **66**, 2693 (1991).
5. M. Kasevich, S. Chu, *Phys. Rev. Lett.* **67**, 181 (1991).
6. P. Szriftgiser, D. Guery-Odelin, M. Arndt, J. Dalibard, *Phys. Rev. Lett.* **77**, 4 (1996).
7. B. Brezger *et al.*, *Phys. Rev. Lett.* **88**, 100404 (2002).
8. M. R. Andrews *et al.*, *Science* **275**, 637 (1997).
9. J. Degert, C. Meier, B. Chatel, B. Girard, *Phys. Rev. A* **67**, 041402 (2003).
10. E. Skovsen, M. Machholm, T. Ejdrup, J. Thøgersen, H. Stapelfeldt, *Phys. Rev. Lett.* **89**, 133004 (2002).
11. C. Petersen, E. Péronne, J. Thøgersen, H. Stapelfeldt, M. Machholm, *Phys. Rev. A* **70**, 033404 (2004).
12. I. S. Averbukh, N. F. Perelman, *Phys. Lett. A* **139**, 449 (1989).
13. O. Knospe, R. Schmidt, *Phys. Rev. A* **54**, 1154 (1996).
14. C. Leichtle, I. S. Averbukh, W. P. Schleich, *Phys. Rev. Lett.* **77**, 3999 (1996).
15. J. A. Yeazell, M. Mallalieu, C. R. Stroud Jr., *Phys. Rev. Lett.* **64**, 2007 (1990).
16. J. A. Yeazell, C. R. Stroud Jr., *Phys. Rev. A* **43**, 5153 (1991).
17. R. M. Bowman, M. Dantus, A. H. Zewail, *Chem. Phys. Lett.* **161**, 297 (1989).
18. M. Gruebele, A. H. Zewail, *J. Chem. Phys.* **98**, 883 (1993).
19. I. Fischer, D. M. Villeneuve, M. J. J. Vrakking, A. Stolow, *J. Chem. Phys.* **102**, 5566 (1995).
20. M. J. J. Vrakking, D. M. Villeneuve, A. Stolow, *Phys. Rev. A* **54**, R37 (1996).
21. I. Fischer, M. J. J. Vrakking, D. M. Villeneuve, A. Stolow, *Chem. Phys.* **207**, 331 (1996).
22. T. Baumert, V. Engel, C. Röttgermann, W. T. Strunz, G. Gerber, *Chem. Phys. Lett.* **191**, 639 (1992).
23. I. S. Averbukh, M. J. J. Vrakking, D. M. Villeneuve, A. Stolow, *Phys. Rev. Lett.* **77**, 3518 (1996).
24. J. Heufelder, H. Ruppe, S. Rutz, E. Schreiber, L. Wöste, *J. Chem. Phys.* **107**, 1 (1997).
25. T. Lohmüller, V. Engel, J. A. Beswick, C. Meier, *J. Chem. Phys.* **120**, 10442 (2004).
26. Z. Bihary, R. Zadayan, M. Karavitis, V. A. Apkarian, *J. Chem. Phys.* **120**, 7576 (2004).
27. W. P. Schleich, *Quantum Optics in Phase Space* (Wiley-VCH, Berlin, 2001).
28. H. Knöckel, B. Bodermann, E. Tiemann, *Eur. Phys. J. D* **28**, 199 (2004).
29. Materials and methods are available as supporting material on Science Online.
30. H. Stapelfeldt, E. Constant, P. B. Corkum, *Phys. Rev. Lett.* **74**, 3780 (1995).
31. A. Assion, M. Geisler, J. Helbing, V. Seyfried, T. Baumert, *Phys. Rev. A* **54**, R4605 (1996).
32. M. Braun, C. Meier, V. Engel, *J. Chem. Phys.* **103**, 7907 (1995).
33. L. W. Ungar, J. A. Cina, *Adv. Chem. Phys.* **100**, 171 (1997).
34. K. Ohmori *et al.*, *Phys. Rev. Lett.* **96**, 093002 (2006).
35. The rotational-level dependence of the predissociation yield of the B state was not taken into account.
36. G. Grégoire *et al.*, *Eur. Phys. J. D* **1**, 187 (1998).
37. C. Nicole *et al.*, *J. Chem. Phys.* **111**, 7857 (1999).
38. Fruitful discussions with A. Beswick, V. Blanchet, V. Engel, T. Lohmüller, and J. Vigué are gratefully acknowledged. This work has been supported by Institute for Molecular Science and by SAKURA (Ministère des Affaires étrangères–Japan Society for the Promotion of Science) international exchange programs, as well as by Grant-in Aid from the Ministry of Education, Culture, Sports, Science and Technology of Japan (15204034, and Priority Area: “Control of Molecules in Intense Laser Fields”) and by Calcul en Midi-Pyrénées (Toulouse) and Centre Informatique National de l’Enseignement Supérieur (Montpellier) computer facilities.

#### Supporting Online Material

www.sciencemag.org/cgi/content/full/311/5767/1589/DC1

Materials and Methods

Figs. S1 and S2

References

11 October 2005; accepted 3 January 2006

10.1126/science.1121240

# MOSFET-Embedded Microcantilevers for Measuring Deflection in Biomolecular Sensors

Gajendra Shekhawat,<sup>1,2\*</sup> Soo-Hyun Tark,<sup>3</sup> Vinayak P. Dravid<sup>1,2,3\*</sup>

A promising approach for detecting biomolecules follows their binding to immobilized probe molecules on microfabricated cantilevers; binding causes surface stresses that bend the cantilever. We measured this deflection, which is on the order of tens of nanometers, by embedding a metal-oxide semiconductor field-effect transistor (MOSFET) into the base of the cantilever and recording decreases in drain current with deflections as small as 5 nanometers. The gate region of the MOSFET responds to surface stresses and thus is embedded in silicon nitride so as to avoid direct contact with the sample solution. This approach, which offers low noise, high sensitivity, and direct readout, was used to detect specific binding events with biotin and antibodies.

The microcantilever detection approach has attracted considerable attention as a means of label-free detection of biomolecules (1–6) in recent years. The specific biomolecular binding between ligands and receptors on the surface of a microcantilever beam results in physical bending of the beam by some tens of nanometers (2–6). The origin of this nanomechanical bending of such a hybrid structure is driven by a change in the surface stress caused when ligands bind to receptors, which leads to a differential bending moment.

The prevailing methods for measuring the microcantilever bending involve optical (1–6), piezoresistive (7–13), and capacitance (14) detection technologies, but each method has some limitations. For example, Majumdar and co-

workers (6) have developed a microcantilever array for multiplexed biomolecular analysis based on a two-dimensional (2D) charge-coupled device (CCD) optical readout to monitor the microcantilever deflection. Optical detection systems are less amenable to monolithic integration and are not readily amenable to massively parallel and highly multiplexed detection because of difficulties in laser alignment and power management. Also, optical detection systems have limited use in situations of turbid or opaque fluidic and smoky environment where light scattering can compromise detection.

Recently, piezoresistive detection (7–13) has emerged as an alternative to optical detection because it is compatible with aqueous media and allows parallel microcantilever arrays to be implemented for detecting multiple analytes at the same time. However, because the piezoresistors cover a large length of the cantilever and high doping levels are required, the stress measurement is not localized. Thus, piezoresistive detection suffers from inevitable thermal and

electronic noise, thermal drifts, nonlinearity in piezo-response, conductance fluctuation noise (usually called flicker or  $1/f$  noise), cycle fatigue, and inadequate sensitivity to very small cantilever deflections. Moreover, microcantilever bending of more than 50 nm is required to detect measurable and reproducible piezoresistance, so this method is insensitive to low concentrations of bimolecular species. Capacitance readout (14) is based on change in the gap due to microcantilever deflection, which results in the change in the capacitance between two conductor plates. Capacitance readout suffers from inevitable interference with the variations in the dielectric constant of the fluidic media.

Here, we report the use of 2D microcantilever arrays with geometrically configured metal-oxide semiconductor field-effect transistors (MOSFETs) embedded in the high-stress region of the microcantilevers to measure deflections induced by biomolecular binding. Finite-element modeling was used to optimize the change in the drain current of the MOSFETs buried in the microcantilevers.

FET-based stress sensors are widely reported for micromechanical devices such as accelerometers, resonators, and parallel cantilevers for scanning probe microscopy, as well as for residual stress measurements (15–20). When a microcantilever bends as a result of adsorption-induced surface stress, modulation of the channel current underneath the gate region results from altered channel mobility of the transistor due to increased channel resistance. As fixed biased voltages are applied on the gate and source-drain region of the transistor, any change in channel mobility will result in change in the drain current of the transistor. Apart from a decrease in channel conductivity, the channel mobility is also affected by the generation of trap states and band structure alteration. However, these stress sensors have not been configured for high sensitivity for small

<sup>1</sup>International Institute for Nanotechnology, <sup>2</sup>NUANCE Center, <sup>3</sup>Department of Materials Science and Engineering, Northwestern University, Evanston, IL 60208, USA.

\*To whom correspondence should be addressed. E-mail: g-shekhawat@northwestern.edu; v-dravid@northwestern.edu

changes in the drain current, nor used for nano-mechanical biomolecular sensor applications. Because MOSFETs and contact pads are passivated with a thin coating of silicon nitride, they are inherently protected from any environmental influence; thus, their performance is not compromised by contact with gases or corrosive liquids such as saline solution.

The MOSFET-embedded microcantilever detection approach is illustrated in Fig. 1. To achieve high sensitivity, we must detect deflections as small as 5 to 10 nm (Table 1). The MOSFETs were engineered for optimal source-drain doping concentration and depth, channel doping, and transistor width/length ratio, taking into account their location at a high-stress region (the cantilever base) (21) and their geometrical configuration (i.e., thickness and length of the cantilever). The optimized design minimizes the electronic noise by (i) selecting localized doping regions on moderately resistive Si cantilevers (10 to 15 ohm-cm) to reduce unwanted noise due to carriers; (ii) precisely controlling the doping region thickness, width, and carriers to optimize the mobility; (iii) having a sharp dopant step profile; and (iv) using a large gate area to suppress  $1/f$  noise. The optimized MOSFET-embedded microcantilevers exhibit measurable, consistent, and reproducible change in the drain current, even for deflections as small as 5 nm.

The microcantilevers were fabricated from SOI (silicon-on-insulator) wafers with a buried oxide etch-stop layer (2.5  $\mu\text{m}$ ) and an epitaxial silicon layer (1.5  $\mu\text{m}$ ). Initially,  $50 \times 1$  cantilever arrays were fabricated with the standard microelectromechanical systems (MEMS) technology (22).

Embedded n-type MOSFET transistors were fabricated on each individual microcantilever by the standard complementary MOS (CMOS) approach, wherein the transistors were located at the rear part of the cantilever where surface stress is the highest (21). Once the process was completed and the MOSFETs were tested for their functionality, microcantilever shapes were defined. Metal contacts to the gate, source, and drain of individual microcantilevers were then made by contact lithography. Finally, the 2.5- $\mu\text{m}$  oxide layer was etched to release the microcantilevers from the top. The transistor design process was simplified with only four masks and minimal process steps for ease of fabrication.

Scanning electron microscopy (SEM) images of one pair of identical cantilevers from an initial  $50 \times 1$  microcantilever array are shown in Fig. 2A. The pair consists of one microcantilever coated with a thin film of gold for immobilization of probe molecules, typically with thiol chemistry, and the other is uncoated and acts as the reference. The differential drain current between the sensing and the reference microcantilevers, which further minimizes systematic noise and environmental perturbations, forms the basis for the MOSFET electronic detection (Fig. 1). The differential signal can be fed into a CMOS-based differential amplifier for electronic

readout at the chip level for future development. A magnified view (Fig. 2B) shows the contact leads and the physical separation of the Cr/Au layer and the contacts. MOSFET-embedded microcantilevers with thickness of 1.5 to 2  $\mu\text{m}$  and length ranging from 200 to 300  $\mu\text{m}$  were fabricated. In each case, the separation between the reference and sensing microcantilevers was about 250  $\mu\text{m}$  for simplicity, the transistor was located about 2 to 4  $\mu\text{m}$  from the cantilever base, and the width/length ratio of source and drain was around 10 to allow for high transconductance. The resonance frequency of the MOSFET-embedded microcantilevers was around 100 to 150 kHz. Each array was designed to have identical sensor (i.e., Cr/Au-coated) and  $\text{SiN}_x$  reference microcantilevers for differential output to

minimize systematic noise and possible false positives. The residual stress that may be introduced by applying a thin layer (30 nm) of gold coating on one side of the cantilever does not create a notable difference in MOSFET current-voltage characteristics when compared with those of  $\text{SiN}_x$  reference cantilevers.

We validated the drain current sensitivity of MOSFET-embedded microcantilevers to bending with the use of a high-resolution nanomanipulator with a vertical ( $z$ -axis) resolution of  $<5$  nm. As the nanomanipulator bent the cantilever downward in steps of 5 nm, the corresponding current-voltage ( $I$ - $V$ ) characteristics were acquired at a fixed gate bias of 5 V in air. We observed (Fig. 3A) a decrease in drain current of 0.1 to 0.2 mA per nanometer of microcantilever

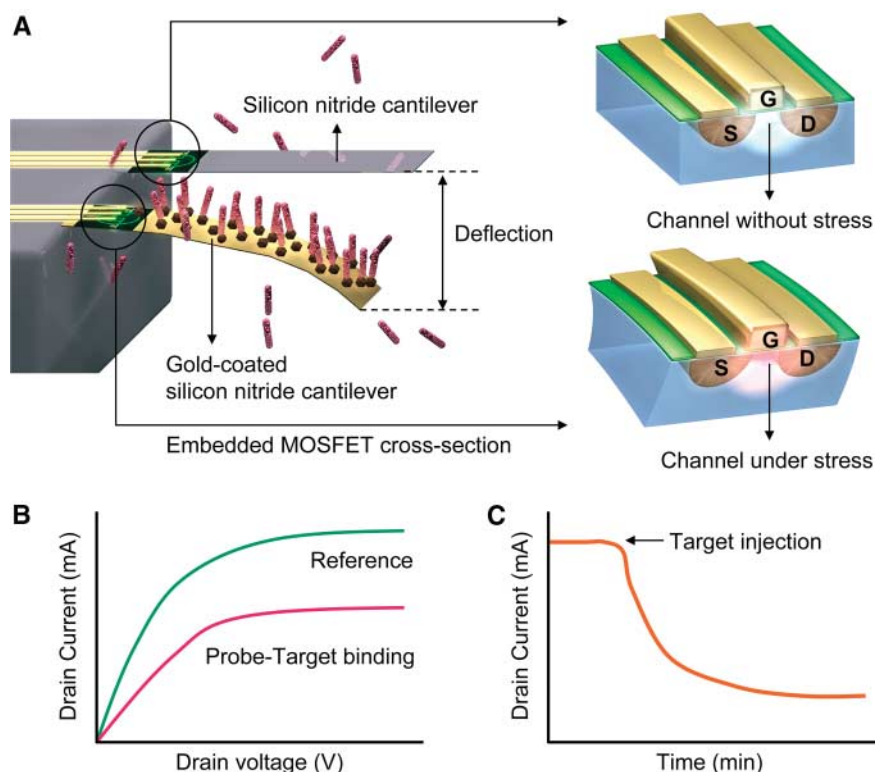


**Fig. 1.** (A) Schematic of the interaction between probe and target molecules on an embedded-MOSFET cantilever system. The silicon nitride cantilever is a reference, and the gold-coated one is used as a sensing cantilever. Specific biomolecular interactions between receptor and target bend the cantilever. Magnified view of embedded MOSFET in cross section shows stressed gate region when cantilever bends, resulting in change of drain current due to conductivity modulation of the channel underneath the gate. (B) Schematic of change in a MOSFET drain current upon probe-target binding. (C) Change in drain current over time due to deflection of a microcantilever.

**Table 1.** A few examples showing conversion of the probe-target biomolecular interactions into nanomechanical responses of microcantilevers (ssDNA, single-stranded DNA; fPSA, free prostate-specific antigen).

Probe-target system	Target molecule concentration	Deflection magnitude (nm)	References
Biotin-streptavidin	100 nM (6 $\mu\text{g}/\text{ml}$ )	50	(1)
Biotin-neutravidin	25 $\mu\text{g}/\text{ml}$	20	(2)
ssDNA hybridization	40 $\mu\text{g}/\text{ml}$ (3 $\mu\text{M}$ )	15	(2)
ssDNA hybridization	500 nM	10	(2)
PSA antibody-fPSA	6 ng/ml	20	(3)

deflection. We note that the drain current changes by almost one order of magnitude between a few nanometers and 150 nm of microcantilever bending. The bending results indicate that the MOSFET deflection sensitivity is of the same order as that of optical detection, as inferred from the prior literature [shown in Table 1 and (3–6)], and is higher than that of existing active and passive detection technologies by one to two orders of magnitude (7–14).

Moreover, MOSFETs have large signal-to-noise (S/N) ratios caused by the large change in drain current relative to the concomitant small noise density (Fig. 3B). The three curves show  $1/f$  or flicker noise—the dominant source of noise in MOSFETs at low frequencies—at three different voltages (23, 24). The current noise of 40 to 60 nA, which is calculated by integrating the spectral power density over  $1/f$  bandwidth for different gate voltages, is lower than the reported value of  $2.7 \mu\text{V}$  for a piezoresistance-based microcantilever-type sensor (25). Given that MOSFET current sensitivity is around 0.1 to 0.2 mA per nanometer of cantilever deflection, a low detection limit can be readily achieved with a large S/N ratio. The noise density could likely be further reduced in future generations of these devices by standard processing steps that would optimize doping concentration and minimize the interface traps.

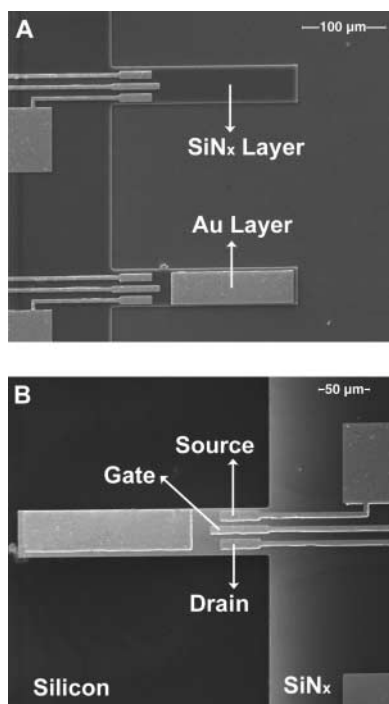


**Fig. 2.** (A) SEM image of two identical cantilevers (from a  $50 \times 1$  array) displaying embedded MOSFET and geometry of the gold-coated and  $\text{SiN}_x$  cantilever beam pair; each cantilever is about 250  $\mu\text{m}$  long, 1.5  $\mu\text{m}$  thick, and 50  $\mu\text{m}$  wide. (B) Details of MOSFET location on cantilever beam, which is released by etching a 2.5- $\mu\text{m}$  sacrificial oxide layer.

Electronic measurements of the transistor characteristics revealed that the observed changes in the drain current at gate bias and while sweeping the drain voltage demonstrate the modulation of channel current with surface stress due to microcantilever bending. The large change in drain current results from the modulation of channel mobility because of surface stress, which increases the channel resistance. The mobility change may also arise from the changes in the interface charge densities, generation of trap states, band structure alteration, and generation of shallow defects due to localized bending stress.

For biomolecular binding experiments, the MOSFET-embedded microcantilevers were cleaned sequentially in acetone, isopropanol-2, and methanol for 10 min each, followed by ultraviolet cleaning for 25 min. They were then functionalized with DTSSP [3,3'-dithiobis (sulfosuccinimidylpropionate), Pierce Chemical Co.], a linker molecule involved in immobilizing streptavidin and antibodies to the gold-coated microcantilever surface. Streptavidin (Pierce) was

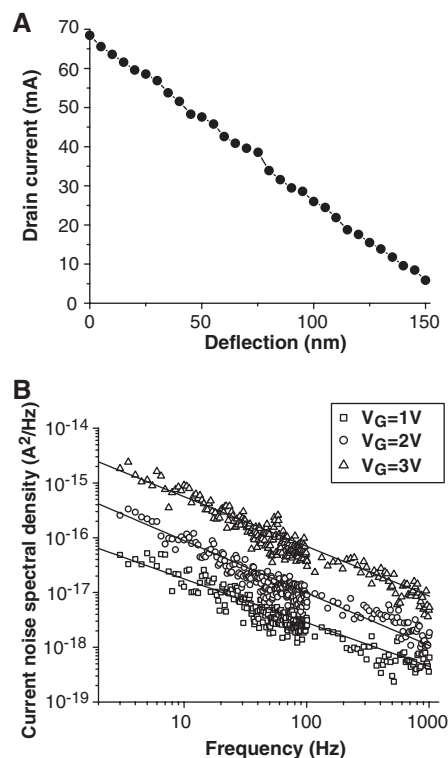


**Fig. 3.** (A) Plot of embedded MOSFET drain current with physical bending of a microcantilever by a nanomanipulator, in step size intervals of 5 nm. The decrease in drain current was 0.1 to 0.2 mA/nm of cantilever deflection. (B) Current noise power spectral densities measured from an embedded MOSFET at different gate voltages and at constant current level, which is inversely proportional to frequency. Current noise power spectral density was measured using a previously described setup (24) with a current preamplifier (DL Instruments, model 1211). The spectra show very low noise level in drain current, supporting high current sensitivity of the device. The drain voltage was fixed at 1 V.

later immobilized on the microcantilever surface by incubating overnight in a streptavidin solution (10  $\mu\text{g}/\text{ml}$ ) prepared with phosphate-buffered sa-

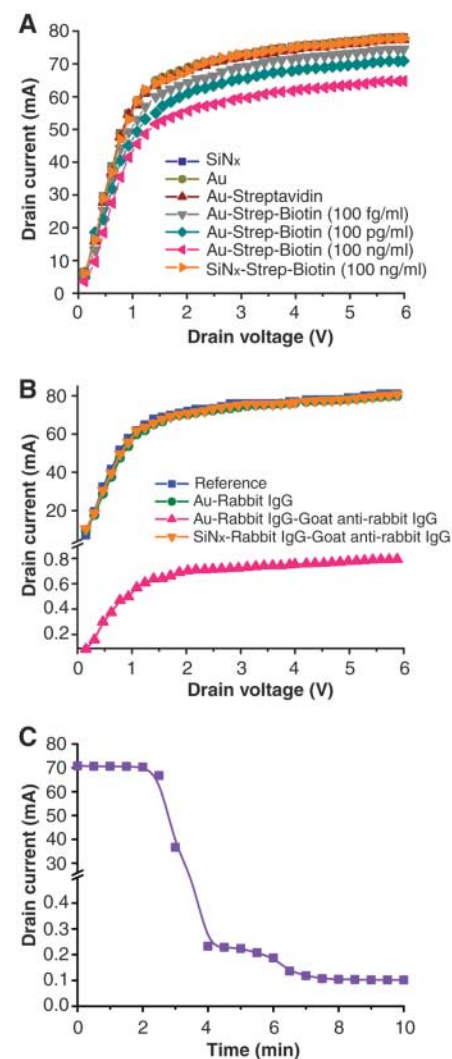


**Fig. 4.** (A)  $I_D$  versus  $V_D$  characteristics of gold-coated cantilever immobilized with streptavidin (10  $\mu\text{g}/\text{ml}$ ) immersed in PBS. The experiment was carried out to check whether the presence of ions caused any bending of the cantilever beam. Negligible change in drain current is observed on the cantilever coated with streptavidin (10  $\mu\text{g}/\text{ml}$ ) in absence of ligands (biotin). When biotin (100 fg/ml to 100 ng/ml) is added, current decreases as concentration increases; this is indicative of cantilever bending. No drain current decrease is observed in the silicon nitride reference cantilever, indicating no probe-target binding. (B) Measured  $I_D$  versus  $V_D$  characteristics for embedded n-MOSFET transistor at  $V_G = 5$  V. There is negligible change in drain current on a cantilever coated with rabbit IgG (0.1 mg/ml) in absence of secondary antibody. When goat antibody to rabbit IgG (0.1 mg/ml) is added, a change in drain current of almost two orders of magnitude is observed, indicative of cantilever bending. (C) Interaction of rabbit IgG and goat antibody to rabbit IgG over time at a fixed drain voltage of 2 V.

line (PBS, pH = 7.4). This immobilization method provides a tight streptavidin layer with uniform density on gold for efficient binding of biotin. All of the nonspecific binding sites were blocked with bovine serum albumin (BSA). For detection experiments, the functionalized microcantilevers were exposed to target biotin concentrations (in PBS) of 100 fg/ml, 100 pg/ml, and 100 ng/ml.

MOSFET transistors were passivated with a thin coating of silicon nitride (30 nm), and electrical contacts were isolated for the binding measurements in the fluidic environment. The measured drain current ( $I_D$ ) versus drain voltage ( $V_D$ ) characteristics for the n-MOSFET-embedded transistor, at gate voltage  $V_G = 5$  V, show a negligible change in  $I_D$  (Fig. 4A) when the streptavidin-immobilized gold microcantilevers are immersed in PBS. Microcantilever bending as a result of streptavidin-biotin binding leads to decreases in  $I_D$  as the concentration of biotin increases from 100 fg/ml to 100 ng/ml. The bending results from an increase in compressive stress, which in turn results from the repulsive electrostatic or steric intermolecular interactions (2–6) or from changes of the hydrophobicity of the surface (1–6). No drain current change was seen in  $\text{SiN}_x$  cantilevers with biotin, where no binding events occurred.

Similar experiments were performed for detection of goat antibodies [secondary immunoglobulin G (IgG)] by rabbit antibodies (primary IgG) with the embedded MOSFET. After the cleaning procedure, the MOSFET-embedded microcantilevers were first functionalized with DTSSP as a linker and then incubated overnight in rabbit IgG (0.1 mg/ml, Pierce) prepared in PBS for immobilization. BSA was again used as an agent to block nonspecific binding sites. The functionalized microcantilevers were exposed to goat antibody to rabbit IgG (0.1 mg/ml in PBS) for binding experiments.

The measured  $I_D$  versus  $V_D$  characteristics for  $V_G = 5$  V (Fig. 4B) again showed no change in the drain current for the  $\text{SiN}_x$  cantilever and negligible change for the gold-coated cantilever with rabbit IgG immersed in PBS. When goat antibody to rabbit IgG (0.1 mg/ml) was introduced, a change in  $I_D$  of almost two orders of magnitude was observed, which is indicative of microcantilever bending as a result of antibody–secondary antibody binding. The  $\text{SiN}_x$  reference cantilever remained the same after injecting the target. The large change in  $I_D$  with time is shown in Fig. 4C; steady-state saturation is achieved when molecular and surface interactions are completed.

The MOSFET detection method offers a number of advantages over traditional piezoresistive or capacitive sensor elements because of its small size, high sensitivity, and uncomplicated current measurement as well as its full and seamless compatibility with direct monolithic integration for application-specific integrated circuits. Moreover, the small channel lengths of MOSFET devices provide more localized stress measurements.

MOSFET-embedded microcantilever detection should allow for massively parallel on-chip signal sensing, multiplexing, and remote addressability via on-chip integration of radio-frequency elements as well as photovoltaics for local power supply.

#### References and Notes

- R. Raiteri, M. Grattarola, H. J. Butt, P. Skladal, *Sens. Actuators B* **79**, 115 (2001).
- G. Wu *et al.*, *Proc. Natl. Acad. Sci. U.S.A.* **98**, 1560 (2001).
- G. Wu *et al.*, *Nat. Biotechnol.* **19**, 856 (2001).
- J. Fritz *et al.*, *Science* **288**, 316 (2000).
- N. V. Lavrik, M. J. Sepaniak, P. G. Datskos, *Rev. Sci. Instrum.* **75**, 2229 (2004).
- M. Yue *et al.*, *J. Microelectromech. Syst.* **13**, 290 (2004).
- A. Boisen, J. Thaysen, H. Jensenius, O. Hansen, *Ultramicroscopy* **82**, 11 (2000).
- H. Jensenius *et al.*, *Appl. Phys. Lett.* **76**, 2615 (2000).
- R. Marie, H. Jensenius, J. Thaysen, C. B. Christensen, A. Boisen, *Ultramicroscopy* **91**, 29 (2002).
- S. C. Minne *et al.*, *Appl. Phys. Lett.* **72**, 2340 (1998).
- S. C. Minne, S. R. Manalis, C. F. Quate, *Appl. Phys. Lett.* **67**, 3918 (1995).
- D. R. Baselt, G. U. Lee, R. J. Colton, *J. Vac. Sci. Technol. B* **14**, 789 (1996).
- D. R. Baselt, G. U. Lee, K. M. Hansen, L. A. Chrisey, R. J. Colton, *Proc. IEEE* **85**, 672 (1997).
- C. L. Britton *et al.*, *Ultramicroscopy* **82**, 17 (2000).
- A. Hamada, T. Furusawa, N. Saito, E. Takeda, *IEEE Trans. Electron Devices* **38**, 895 (1991).
- R. C. Jaeger, J. C. Suhling, R. Ramani, A. T. Bradley, J. P. Xu, *IEEE J. Solid-State Circuits* **35**, 85 (2000).
- Y. J. Yee, J. U. Bu, K. J. Chun, J. W. Lee, *J. Microchem. Microeng.* **10**, 350 (2000).
- T. Akiyama *et al.*, *J. Vac. Sci. Technol. B* **18**, 2669 (2000).
- D. Lange, C. Hagleitner, C. Herzog, O. Brand, H. Baltes, *Sens. Actuators A* **103**, 150 (2003).
- T. Akiyama, U. Staufner, N. F. de Rooij, *Rev. Sci. Instrum.* **73**, 2643 (2002).
- R. Bashir, A. Gupta, G. W. Neudeck, M. McElfresh, R. Gomez, *J. Microchem. Microeng.* **10**, 483 (2000).
- C. Liu, *Foundations of MEMS* (Pearson Prentice Hall, Upper Saddle River, NJ, 2005).
- V. Dessard, B. Iniguez, S. Adriaensen, D. Flandre, *IEEE Trans. Electron Devices* **49**, 1289 (2002).
- A. Blaum, O. Pilloud, G. Scalea, J. Victory, F. Sischka, in *Proceedings of the 2001 International Conference on Microelectronic Test Structures* (IEEE, Piscataway, NJ, 2001), pp. 125–130.
- P. A. Rasmussen, J. Thaysen, O. Hansen, S. C. Eriksen, A. Boisen, *Ultramicroscopy* **97**, 371 (2003).
- Supported by NSF Electrical and Communications System grant ECS-0330410 and Defense Advanced Research Projects Agency grant F30602-01-2-0540. This work made use of the Microfabrication Applications Laboratory at the University of Illinois, Chicago, the Center for Nanophase Materials Science at Oak Ridge National Laboratory, and the NUANCE center facilities at Northwestern University. We thank R. Lajos, H. Zeng, and A. Feinerman for process assistance and support; T. Thundat, D. Ramaya, K. Hansen, and I. Lee for assistance in immobilization of antibodies; and A. Srivastava for assistance in noise measurements.

#### Supporting Online Material

www.sciencemag.org/cgi/content/full/1122588/DC1

Materials and Methods

References

14 November 2005; accepted 20 January 2006

Published online 2 February 2006;

10.1126/science.1122588

Include this information when citing this paper.

## Broadband Cavity Ringdown Spectroscopy for Sensitive and Rapid Molecular Detection

Michael J. Thorpe, Kevin D. Moll, R. Jason Jones, Benjamin Safdi, Jun Ye\*

We demonstrate highly efficient cavity ringdown spectroscopy in which a broad-bandwidth optical frequency comb is coherently coupled to a high-finesse optical cavity that acts as the sample chamber. 125,000 optical comb components, each coupled into a specific longitudinal cavity mode, undergo ringdown decays when the cavity input is shut off. Sensitive intracavity absorption information is simultaneously available across 100 nanometers in the visible and near-infrared spectral regions. Real-time, quantitative measurements were made of the trace presence, the transition strengths and linewidths, and the population redistributions due to collisions and the temperature changes for molecules such as  $\text{C}_2\text{H}_2$ ,  $\text{O}_2$ ,  $\text{H}_2\text{O}$ , and  $\text{NH}_3$ .

The real-time detection of trace amounts of molecular species is needed for applications that range from detection of explosives or biologically hazardous materials to analysis of a patient's breath to monitor diseases such as renal failure (1) and cystic fibrosis (2). Spectroscopic systems ca-

pable of making the next generation of atomic and molecular measurements will require the following: (i) a large spectral bandwidth, allowing for the observation of the global energy level structure of many different atomic and molecular species; (ii) high spectral resolution for the identification and quantitative analysis of individual spectral features; (iii) high sensitivity for the detection of trace amounts of atoms or molecules and for the recovery of weak spectral features; and (iv) a fast spectral acquisition time, which takes advantage of high sensitivity, for the study of dynamics.

JILA, National Institute of Standards and Technology (NIST) and University of Colorado, and Department of Physics, University of Colorado, Boulder, CO 80309-0440, USA.

\*To whom correspondence should be addressed. E-mail: ye@jila.colorado.edu